

Materials Research Letters

ISSN: 2166-3831 (Online) Journal homepage: www.tandfonline.com/journals/tmrl20

Achieving and stabilizing fine near-equiaxed grains in additively manufactured Ni-superalloys

Zhaowei Wang , Zhuangzhuang Zhang , Yuyang Zhang , Kai Chen, Lin Shi , Lifeng Liu & Wolfgang Pantleon

To cite this article: Zhaowei Wang , Zhuangzhuang Zhang , Yuyang Zhang , Kai Chen, Lin Shi , Lifeng Liu & Wolfgang Pantleon (2026) Achieving and stabilizing fine near-equiaxed grains in additively manufactured Ni-superalloys, Materials Research Letters, 14:10, 1319-1327, DOI: 10.1080/21663831.2026.2713907

To link to this article: https://doi.org/10.1080/21663831.2026.2713907

© 2026 The Author(s). Published by Informa UK Limited, trading as Taylor & Francis Group.

View supplementary material

Published online: 07 Aug 2026.

Submit your article to this journal

Article views: 648

View related articles

View Crossmark data

Full Terms & Conditions of access and use can be found at https://www.tandfonline.com/action/journalInformation?journalCode=tmrl20

MATER. RES. LETT.
2026, VOL. 14, NO. 10, 1319–1327
https://doi.org/10.1080/21663831.2026.2713907

MATERIALS RESEARCH LETTERS
Taylor & Francis by informa

ORIGINAL REPORTS

OPEN ACCESS Check for updates

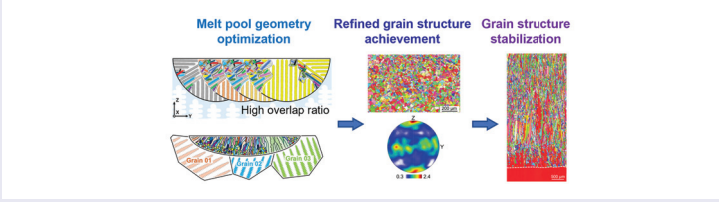
Achieving and stabilizing fine near-equiaxed grains in additively manufactured Ni-superalloys

Zhaowei Wang[a], Zhuangzhuang Zhang[a], Yuyang Zhang[a], Kai Chen [a], Lin Shi[b], Lifeng Liu[c] and Wolfgang Pantleon [d]

[a]Center for Advancing Materials Performance from the Nanoscale (CAMPNano), State Key Laboratory for Mechanical Behavior of Materials, Xi'an Jiaotong University, Xi'an, People's Republic of China; [b]Institute of Surface-Earth System Science, School of Earth System Science, Tianjin University, Tianjin, People's Republic of China; [c]Taishan Fiberglass Inc., Tai'an, People's Republic of China; [d]Department of Civil and Mechanical Engineering, Technical University of Denmark, Kongens Lyngby, Denmark

ABSTRACT

Site-specific grain-structure control is desirable for turbine blades with region-specific performance requirements. Here, we demonstrate that a columnar-to-equiaxed transition can be initiated in electron-beam additive manufacturing within individual melt pools and retained through controlled overlap ratio and melt pool geometry. A high overlap ratio with shallow melt pools increases grain density and suppresses competitive dendritic growth, yielding near-equiaxed grains with an average size of $\sim 30\ \mu$m on single-crystalline substrates. A tailored heat-treatment protocol incorporating optimized recovery annealing relieves stresses while preventing recrystallization, thereby stabilizing the refined microstructure. This strategy enables grain structure design without altering established alloy compositions.



ARTICLE HISTORY
Received 16 April 2026

KEYWORDS
Ni-based superalloys; electron-beam melting additive manufacturing; grain structure manipulation; heat treatment; columnar-to-equiaxed transition

1. Introduction

The desired grain structure for Ni-based superalloy turbine blades is site-dependent. Blade tips operate under high centrifugal stresses at elevated temperatures ($\sim$1000°C), requiring columnar grains or even single crystals to enhance creep resistance [1,2]. In contrast, blade roots are typically exposed to cyclic vibrations and loads at lower temperatures (650–750°C), and thus fine near-equiaxed grains are more favorable [3,4]. Grain refinement can enhance the fatigue life significantly in both forgeable [5] and unforgeable [6] superalloys. However, fabricating site-specific microstructures remains challenging. Conventional casting offers limited flexibility in grain-structure control, and is generally optimized to produce fully columnar or single-crystalline blades. Although blade roots can be strengthened through external treatments such as shot peening or laser shock peening [7], these methods are costly, and their effectiveness often degrades over time. Severe plastic deformation after casting followed by subsequent heat treatment can refine the grain structure of forgeable superalloys [8], but this strategy does not work for unforgeable precipitation-strengthened superalloys with high volume fraction of γ' precipitates. Alternatively, additive manufacturing (AM), with its unique layer-wise deposition nature, offers promising potential for site-specific grain structure design and manipulation [9–12].

Nevertheless, achieving a uniform, fine equiaxed grain structure on single-crystalline substrates by AM remains highly challenging. Although hatch-overlap-induced microstructure control has been widely reported

CONTACT Kai Chen kchenlbl@gmail.com Center for Advancing Materials Performance from the Nanoscale (CAMPNano), State Key Laboratory for Mechanical Behavior of Materials, Xi'an Jiaotong University, Xi'an, Shaanxi 710049, People's Republic of China

Supplemental data for this article can be accessed online at https://doi.org/10.1080/21663831.2026.2713907.

© 2026 The Author(s). Published by Informa UK Limited, trading as Taylor & Francis Group.
This is an Open Access article distributed under the terms of the Creative Commons Attribution-NonCommercial License (http://creativecommons.org/licenses/by-nc/4.0/), which permits unrestricted non-commercial use, distribution, and reproduction in any medium, provided the original work is properly cited. The terms on which this article has been published allow the posting of the Accepted Manuscript in a repository by the author(s) or with their consent.

in laser-based AM, previous studies have largely focused on conventionally printable alloys (e.g. IN718), treating overlap ratio primarily as an empirical process parameter for grain refinement or texture control. In most cases, increasing overlap promotes remelting and epitaxial columnar growth, whereas reducing overlap weakens epitaxy and facilitates grain refinement or the formation of stray grains [13–16]. However, the steep thermal gradients intrinsic to AM strongly favor epitaxial solidification. Although Marangoni convection [17], inter-track interactions [18], and heat accumulation locally perturb solidification conditions [19], they generally produce only sporadic stray grains within a predominantly columnar microstructure. Disrupting epitaxial growth on a single-crystalline substrate therefore remains challenging. Moreover, even when equiaxed grains are obtained, tailored post-processing is still required to suppress recrystallization and grain coarsening [20,21].

In this work, a fine near-equiaxed microstructure is realized on single-crystalline substrates via electron-beam powder bed fusion using an exceptionally high overlap ratio with a shallow melt pool. A customized heat-treatment protocol is developed to effectively relieve residual stresses, thereby suppressing recrystallization and grain coarsening. This study establishes a facile yet robust AM-enabled strategy for the repair and remanufacturing of Ni-based superalloy turbine blade roots through site-specific grain-structure programming.

2. Kinetic considerations

A kinetic analysis is conducted to identify the overlap ratio and melt-pool morphology favoring near-equiaxed grain formation. For single-track melting, dendrite growth is governed by melt-pool geometry and substrate crystallography. Dendritic growth along crystallographic direction $[uvw]$ occurs with velocity

$$|V_{[uvw]}| = \frac{|V_n|}{\cos \psi_{[uvw]}} \tag{1}$$

determined by the velocity V_n of the solidification front and the angle $\psi_{[uvw]}$ between the normal of the solidification front and the $[uvw]$ direction [22]. The corresponding thermal gradient is given by the thermal gradient G_n normal to the solidification front [23].

$$|G_{[uvw]}| = |G_n| \cos \psi_{[uvw]}. \tag{2}$$

For Ni-based superalloys, primary dendrites grow along [001], with secondary arms along [100] and [010], forming a structure with four-fold symmetry. Previous modeling indicates that large V[001] and reduced G[001], achievable at larger ψ[001], promote the columnar-to-equiaxed transition and thus near-equiaxed structures [23–25].

However, single-crystalline blades are typically oriented with [001] normal to the build plane. Under such conditions, ψ[001] is small near the melt-pool center, favoring epitaxial columnar growth. Along the melt pool sidewalls, dendrites preferentially grow with one of their $<100>$ directions parallel to the [100] or [010] directions. Although they appear perpendicular to the substrate dendrites, their crystallographic orientation remains equivalent and therefore does not generate stray grains or contribute to grain refinement.

A columnar-to-equiaxed transition becomes more likely when $<100>$ is inclined to the local solidification-front normal. A higher angle ψ[001] causes a lower G/V ratio

$$\frac{|G_{[hkl]}|}{|V_{[hkl]}|} = \frac{|G_n|}{|V_n|}\cos^2 \psi_{[hkl]} < \frac{|G_n|}{|V_n|} \tag{3}$$

promoting equiaxed stray-grain nucleation and the columnar-to-equiaxed transition [23,25]. This is the case for the intermediate zones between different $<100>$ growth directions [22], as well as near melt pool bottoms located in interdendritic regions, where local fusion line perturbations arise from microsegregation [26]. While the density of fusion line perturbations is constrained by the dendrite spacing in the substrate and therefore difficult to modify, increasing the overlap ratio between adjacent melting tracks offers an effective strategy to increase the density of stray grains (Figure 1(a and b)).

In addition to overlap ratio, melt pool morphology critically influences the size and evolution of stray grains. When stray grains are already present in a previously deposited layer, subsequent solidification proceeds on a polycrystalline substrate. If a melt pool spanning several substrate grains is deep, the wide melt pool provides sufficient space for competitive dendritic growth and coarsening, producing thick columnar grains that counteract grain refinement and formation of an equiaxed grain structure (Figure 1(c)). In contrast, a shallow melt pool increases the relative volume fraction of stray grains nucleated near the fusion line and restricts their coarsening, coalescence, and elongation. It also promotes the retention of stray grains formed between differently oriented $<100>$ growth directions (Figure 1(d)).

Under repeated high-overlap deposition, these retained stray grains become part of the growth substrate for subsequent melt tracks. As deposition proceeds, lateral remelting progressively disrupts long-range epitaxial inheritance and increases the crystallographic heterogeneity of the local growth front. Consequently, grain refinement should be regarded as the coupled result of

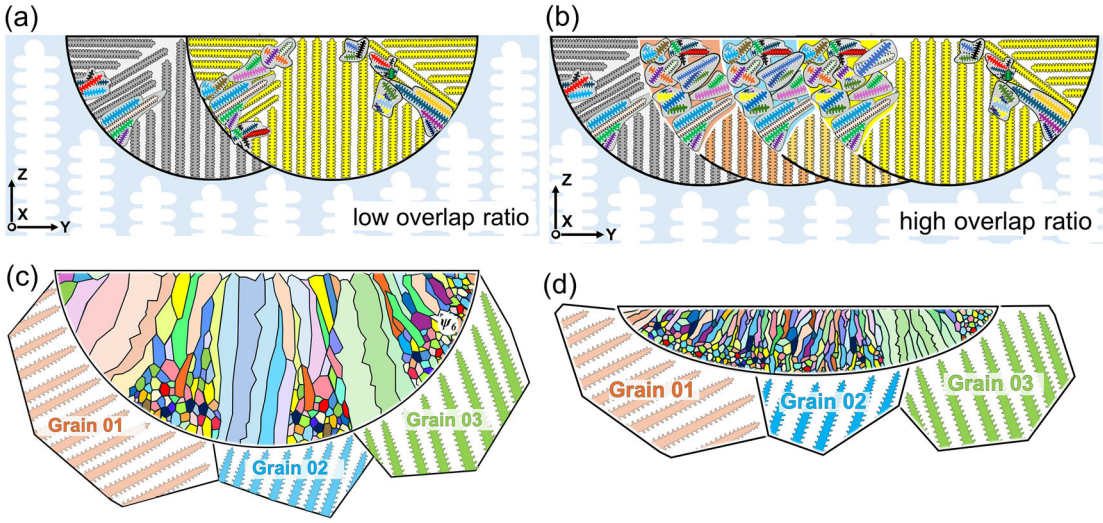


Figure 1. Schematic illustration of the effects of overlap ratio (a vs. b) and melt pool morphology (c vs. d) on the formation and retention of near-equiaxed grains.

preferential stray-grain generation, retention, and progressive disruption of epitaxial inheritance.

3. Results

3.1. Experimental validation

Experimental details are provided in the Supplementary Materials. Process optimization was established through surface melting of directionally solidified DZ125 substrates and subsequently applied to additive manufacturing on directionally solidified DZ125 and single-crystalline DD6 substrates. Both substrates maintain a continuous $<001>$ orientation parallel to the build direction, providing comparable epitaxial growth conditions while representing two technologically relevant substrate architectures (Figure S1). The melt-pool geometry is examined without powder feedstock by fixing the electron-beam power at 400 W while varying the scanning speeds. Single-track melt pools show that increasing scanning speed from 400 mm·s^{-1} to 2500 mm·s^{-1} reduces the melt-pool width from 680 µm to 420 μm and reduces the melt-pool depth from 227 µm to 67 μm (cf. Figure S2 in the Supplementary Materials). At the optimized scanning speed of 2000mm·s^{-1}, the fabricated samples exhibit substantially reduced defect densities, yielding a lack-of-fusion area fraction of $0.03 \pm 0.01\%$, a pore area fraction of $0.03 \pm 0.03\%$, and a crack density of 0.41 ± 0.04 mm^{-1} (Figure S3 and Table S1). Conversely, at 2500 mm·s^{-1}, the melt-pool depth decreases to 67 μm, falling significantly below the powder particle diameter, which induces a marked increase in lack-of-fusion defects ($1.66 \pm 0.13\%$), pore area fraction ($0.33 \pm 0.11\%$), and crack density (0.92 ± 0.24 mm^{-1}) (Figure S3 and Table S1). Consequently, a scanning speed of 2500 mm·s^{-1} is deemed unsuitable.

At 400 W and 2000mm·s^{-1}, single-track melt pools are approximately 500 µm in width and 95 µm in depth; thus, hatch spacings of 300, 200, and 100 µm, correspond to overlap ratios of 40%, 60%, and 80% respectively. Two-dimensional scanning and heat accumulation cause thicker melted layers than single-track melting. With 40% and 60% overlap ratios, shallow melt layers (110–130 μm), as shown in Figures 2(a, d and b, e) remain predominantly epitaxial, with stray grains (highlighted in yellow) occupying only $8 \pm 4\%$ of the cross-sectional area. In contrast, increasing the overlap ratio to 80% results in a thicker melted layer of approximately 150 µm and a clear disruption of epitaxial inheritance. Accordingly, the stray-grain area fraction increases to $62 \pm 15\%$ (Figure 2(c, f)). An orientation map showing the crystallographic direction along the build direction (Z-direction) (Figure 2(f)) according to the inverse pole figure (IPF) reveal two distinct populations of stray grains at 80% overlap ratio: (Type 1) fine near-equiaxed grains with sizes 7.5 µm to 19.9 µm located predominantly near the fusion line, and (Type 2) coarse, slightly columnar stray grains in the central and upper regions of the melted layer, often growing on top of Type 1 stray grains, thereby disrupting epitaxy with the single-crystalline substrate.

To elucidate the influence of electron-beam scanning speed, blocks are fabricated at scanning speeds of 400, 1200, and 2000mm·s^{-1} with constant electron-beam power (400 W). The hatch spacing is adjusted according to the measured melt-pool width (Figure S2) to maintain a melt-pool overlap ratio of approximately 80%, which was further validated by measurements of the melt-pool geometry in the AM-built blocks (Figure S4).

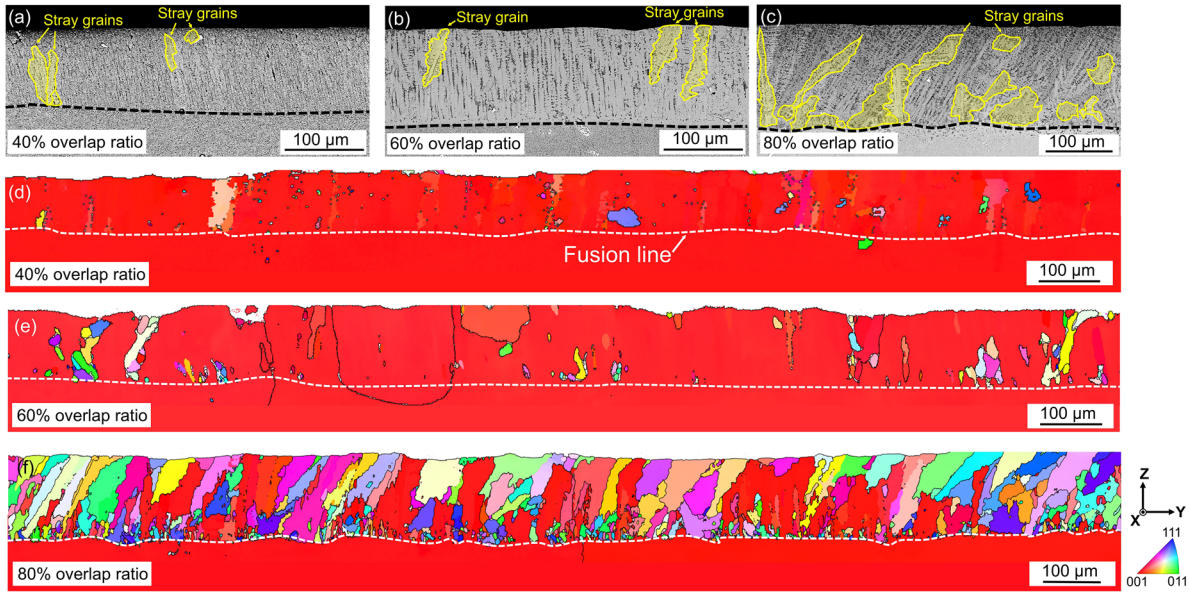


Figure 2. Effect of overlap ratio on grain structure during electron-beam surface melting of directionally solidified DZ125 substrates. (a–c) SEM images of as-melted regions obtained at overlap ratios of 40%, 60%, and 80%, respectively. (d–f) EBSD IPF-Z maps obtained from the 40%, 60%, and 80% overlap conditions.

From the orientation maps (in Figures 3(a–c)), grain size was quantified as the area-weighted equivalent circular diameter. Grain refinement on both sections, YZ and XY, becomes increasingly pronounced as melt-pool sizes decrease. The 001 pole figures for all three specimens in Figures 3(a3–c3) reveal a $< 100 >$ fiber texture progressively weakening with increasing scanning speed, concomitant with grain refinement. The maximum {001} pole-figure intensity decreased from 10.7 ± 0.6 MUD to 2.4 ± 0.3 MUD with increasing overlap ratio. At a scanning speed of 2000mm·s^{-1}, the predominantly near-equiaxed grains exhibit a rather weak $< 100 >$ fiber texture.

Grains exhibit notable elongation along the build direction on the YZ-section, reflecting some residual tendency for columnar growth, while appearing more equiaxed on XY-planes. Grain aspect ratios were quantified on both sections. The cumulative area distributions are shown in Figures 3(d and e). For both sections, the aspect ratios vary only slightly with scanning speed and, hence, melt-pool size. The aspect ratio on YZ (2.8 ± 1.5) is significantly larger than that on XY (1.7 ± 0.6), conforming the visual impression of a slightly elongated grain structure.

Overall, increasing scanning speed within an appropriate range produces narrower and shallower melt pools, leading to significant grain refinement without appreciably altering the grain morphology.

3.2. Microstructure stability

Using optimized parameters (400 W, 2000mm·s^{-1}, 80% overlap), electron-beam AM on a DD6 single-crystalline superalloy substrate produces a refined microstructure with an area-weighted average grain size of 49 ± 29 μm and an area-weighted aspect ratio of 2.7 ± 1.9. A ~750 μm high transitional zone with columnar grains separates the single-crystalline substrate and the slightly elongated polycrystalline region. Above the transitional zone, clusters of fine grains dispersed in vertically banded regions dominate the entire block. Higher-resolution EBSD maps are performed in the polycrystalline region and represented with a boundary map in Figures 4(a2 and a3). The corresponding pole figure of this refined region is provided in Figure S5a, showing that the refined grain layer retains a moderate $< 001 >$ fiber texture. Using the Read–Shockley equation [27], the energy stored in boundaries is estimated with a shear modulus of 70 GPa and a Poisson ratio of 0.3. For the interior boundaries within the grains, a stored energy of 21 kJ/m^3 is obtained, constituting a driving force for recrystallization.

The as-built block is subjected to the standard industrial heat treatment for DZ125, consisting of solutionizing at 1180°C for 2 h followed by 1230°C for 3 h, and subsequent ageing at 1100°C for 4 h. The absence of low angle boundaries within the huge grains in Figure 4(b3) indicates recrystallization is readily initiated under this treatment, followed by grain growth (Figure 4(b2)) and occasional formation of annealing twins (highlighted in

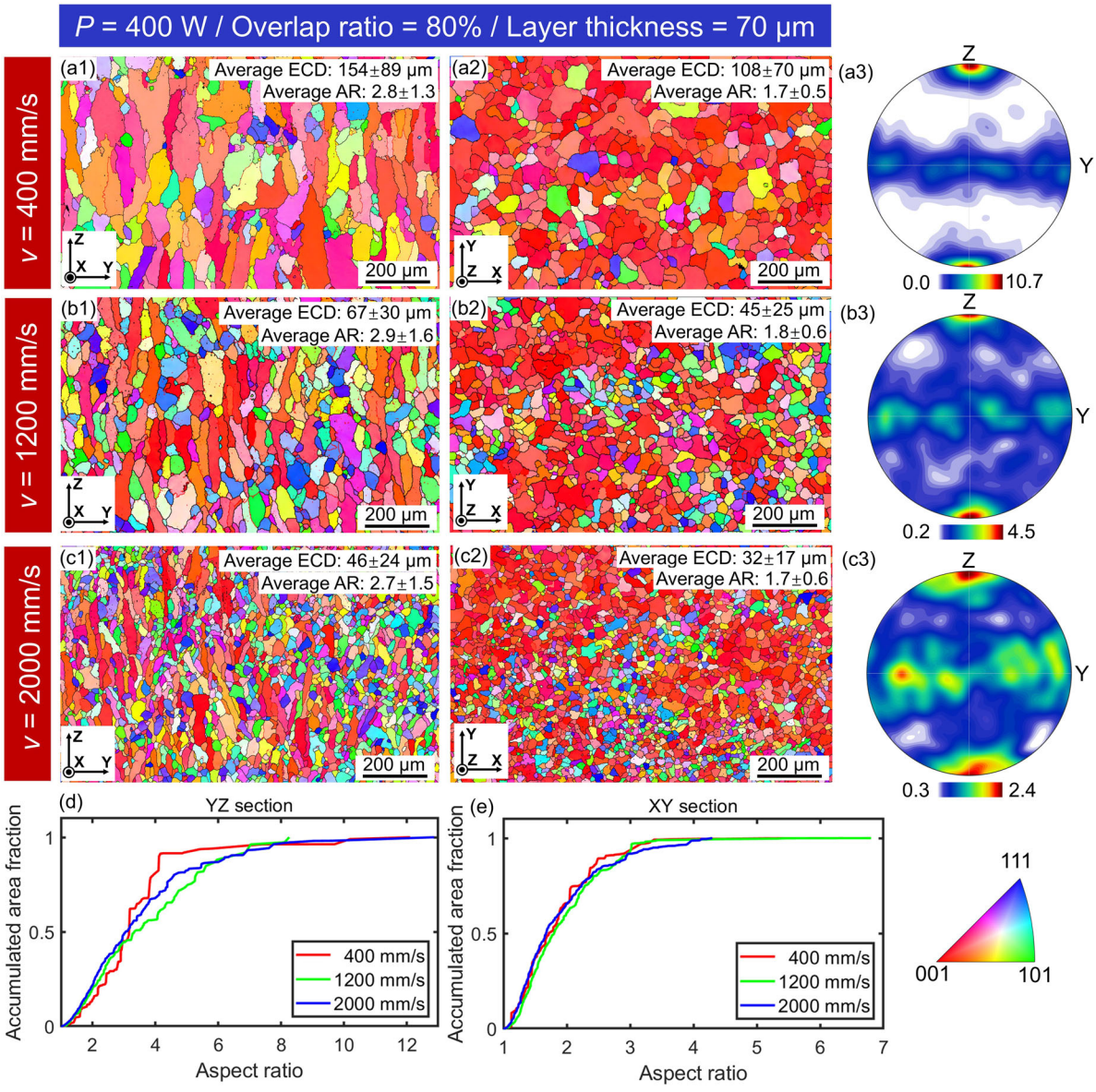


Figure 3. Grain refinement through melt-pool manipulation in additively manufactured DZ125 deposited on directionally solidified DZ125 substrates. (a–c) EBSD IPF-Z maps and 001 pole figures of as-built samples fabricated at different scanning speeds. (d–e) Cumulative area fraction of grain aspect ratio on the YZ- and XY-sections.

Figure 4(b3)). The energy stored in the inner boundaries is reduced to 3.9 kJ/m^3.

Alternatively, an as-built block is exposed to a custom-designed heat-treatment protocol (slightly adjusted from the one in [21,28,29]) comprising a recovery annealing stage with slow ramping from 1100°C to 1230°C over 2 h, followed by the standard solutionizing and ageing treatment. Such tailored heat treatment preserves the refined grain structure, with an average grain size of 51 ± 31 μm (Figure 4(c)) and a moderate $<001>$ fiber texture (Figure S5c). With a low energy of 8.8 kJ/m^3 in the internal boundaries, this microstructure will be much less prone to recrystallization than the as-built microstructure.

4. Discussion

The formation of the refined near-equiaxed microstructure cannot be attributed to overlap ratio or melt-pool morphology alone. Instead, it results from the coupled effects of three sequential processes: (i) preferential stray-grain generation where the CET criterion is locally satisfied; (ii) retention of these newly formed grains by shallow melt pools that suppress competitive dendritic growth; and (iii) progressive disruption of epitaxial inheritance during repeated high-overlap deposition. Within this framework, the primary role of a high overlap ratio is to continuously generate favorable local CET

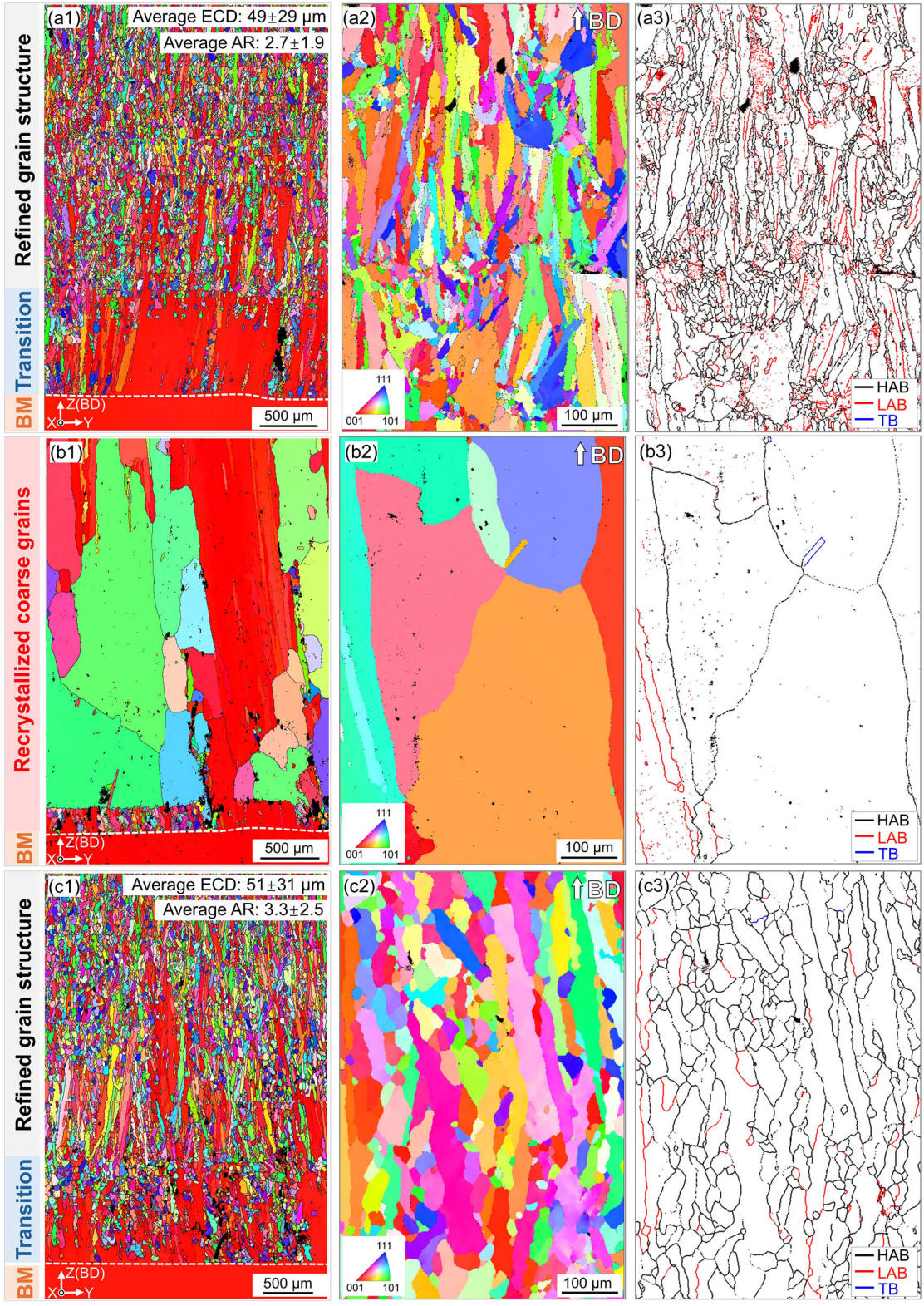


Figure 4. Stabilization of the refined microstructure by tailored heat treatment. EBSD IPF-Z maps of (a) the as-built sample, (b) a sample after standard heat treatment, and (c) a sample after tailored heat treatment. Left: overview maps; middle: enlarged orientation maps; right: corresponding boundary maps. High angle boundaries (HABs) with disorientation angles above 15° are delineated in black, low angle boundaries (LABs) with disorientation angles above 1° in red and twin boundaries (TB, Σ3 boundaries) in blue.

sites rather than directly refine the existing columnar structure.

Retention of newly generated stray grains is governed by competitive dendritic growth during subsequent solidification, which is strongly influenced by melt-pool geometry. In deep melt pools, competitive dendritic growth favors crystallographically preferred grains, reducing stray-grain retention and restoring coarse columnar structures. By contrast, shallow melt pools shorten the dendritic selection distance and restrict competitive grain growth, thereby suppressing grain coarsening. Grain refinement is therefore governed not by maximizing stray-grain generation alone, but by the coupled effects of stray-grain generation, retention, and the progressive disruption of epitaxial inheritance during repeated deposition. This balance simultaneously defines the practical processing window, since excessive reduction in melt-pool depth inevitably compromises interlayer metallurgical bonding and promotes lack-of-fusion defects. Within this window, an average grain size of 32 ± 17 μm is finally achieved, which is well below those reported for non-forgeable Ni-based superalloys [30,31], comparable to the finest grain sizes achieved in forgeable alloys through thermomechanical processing [8,32].

Stabilization of the refined grain structure requires decoupling recovery from recrystallization during subsequent heat treatment. Compositional segregation between dendrite cores and interdendritic regions creates a narrow sub-solvus temperature window that promotes recovery while suppressing recrystallization [21]. The proposed ramping solution treatment (Figure 4) therefore preserves the refined microstructure. Following stray-grain generation, retention, and stabilization, further refinement may be achieved by combining melt-pool engineering strategy with localized alloy chemistry optimization, such as controlled carbon and boron additions [33–36], to enhance heterogeneous nucleation and Zener pinning [37,38]. Nevertheless, compositionally graded microstructures require careful control of interdiffusion kinetics and phase stability to ensure long-term microstructural stability and service reliability.

5. Conclusion

Through systematic analysis of overlap ratio and melt-pool morphology, a strategy is established to achieve fine near-equiaxed grain structures in additively manufactured non-forgeable Ni-based superalloys. On directionally solidified or single-crystalline substrates, a columnar-to-equiaxed transition can be triggered within individual melt pools. A high overlap ratio combined with narrow and shallow melt pools maximizes equiaxed-grain retention and is therefore adopted for block fabrication. The as-built grains are slightly elongated along the build direction but nearly equiaxed in the plane perpendicular to the build direction. Subsequent to deposition, a custom-designed heat-treatment protocol is applied, consisting of slow ramp-up recovery annealing, solutionizing, and then ageing. This treatment effectively relieves residual stresses, reduces stored energy, suppresses recrystallization, and stabilizes the refined grain structure. The present work establishes both a fundamental understanding and a practical framework for grain-structure design in additive manufacturing without altering established alloy compositions, offering a potential route toward the advanced manufacturing and repair of turbine blade roots.

Author contributions

CRediT: **Zhaowei Wang:** Investigation, Visualization, Writing – original draft; **Zhuangzhuang Zhang:** Investigation, Visualization; **Yuyang Zhang:** Visualization; **Kai Chen:** Conceptualization, Funding acquisition, Project administration, Supervision, Writing – review & editing; **Lin Shi:** Investigation; **Lifeng Liu:** Resources; **Wolfgang Pantleon:** Supervision, Validation, Writing – review & editing

Disclosure statement

No potential conflict of interest was reported by the author(s).

Funding

This work is supported by the open research fund of Suzhou Laboratory No. SZLAB-1608-2025-TS040, the National Key Research and Development Program of China under grant number 2023YFB12002, and the National Natural Science Foundation of China (grant number W2411048, 22409160). We also thank Instrumental Analysis Center of Xi'an Jiaotong University and Dr. Chuanwei Fan for technical support.

ORCID

Kai Chen http://orcid.org/0000-0002-4917-4445
Wolfgang Pantleon http://orcid.org/0000-0001-6418-6260

References

[1] Reed RC. The superalloys: fundamentals and applications. Cambridge: Cambridge University Press; 2008.
[2] Pollock TM, Tin S. Nickel-based superalloys for advanced turbine engines: chemistry, microstructure and properties. J Propuls Power. 2006;22(2):361–374. doi:10.2514/1.18239
[3] Mall S, Kim HK, Saladin EC, et al. Effects of microstructure on fretting fatigue behavior of IN100. Mater Sci Eng A. 2010;527(6):1453–1460. doi:10.1016/j.msea.2009.10.068

[4] Yao SL, Zeng XT, Li KS, et al. Fretting fatigue life improvement of nickel-based superalloy GH4169 dovetail slots by deflecting abrasive waterjet peening process. Int J Fatigue. 2023;175:107832. doi:10.1016/j.ijfatigue.2023.107832
[5] Alexandre F, Deyber S, Pineau A. Modelling the optimum grain size on the low cycle fatigue life of a Ni based superalloy in the presence of two possible crack initiation sites. Scr Mater. 2004;50(1):25–30. doi:10.1016/j.scriptamat.2003.09.043
[6] Du B, Yang J, Cui C, et al. Effects of grain size on the high-cycle fatigue behavior of IN792 superalloy. Mater Des. 2015;65:57–64. doi:10.1016/j.matdes.2014.08.059
[7] Zhou G, Zhang Y, Pantleon W, et al. Quantification of room temperature strengthening of laser shock peened Ni-based superalloy using synchrotron microdiffraction. Mater Des. 2022;221:110948. doi:10.1016/j.matdes.2022.110948
[8] Yang P, Huang Y, Guo Q, et al. Obtaining ultra-fine grains by hot deformation without inducing secondary phase pinning grain boundaries in Ni-based superalloy. J Mater Process Technol. 2025;344:119020. doi:10.1016/j.jmatprotec.2025.119020
[9] Raghavan N, Simunovic S, Dehoff R, et al. Localized melt-scan strategy for site specific control of grain size and primary dendrite arm spacing in electron beam additive manufacturing. Acta Mater. 2017;140:375–387. doi:10.1016/j.actamat.2017.08.038
[10] Ramsperger M, Eichler S. Electron beam based additive manufacturing of alloy 247 for turbine engine application: from research towards industrialization. Metall Mater Trans A. 2023;54(5):1730–1743. doi:10.1007/s11661-022-06955-0
[11] Lei Y, Aoyagi K, Chiba A. A method to manipulate non-steady-state columnar-to-equiaxed transition in powder bed fusion additive manufacturing using an electron beam. Acta Mater. 2022;227:117717. doi:10.1016/j.actamat.2022.117717
[12] Wang Z, Liu F, Gao S, et al. Turn nonweldable Ni-superalloys printable and microstructurally controllable. Adv Mater. 2026: e17003. doi:10.1002/adma.202517003
[13] Rodríguez-Barber I, Pérez-Prado MT. Melt pool overlap as a key tool for microstructure design in PBF-LB/M of a Ni-based superalloy: empirical and analytical approaches. Addit Manuf. 2025;109:104901. doi:10.1016/j.addma.2025.104901
[14] Yang Z, Li X, Chang J, et al. On the stray grains in single-crystal Ni-based superalloy by additive manufacturing: formation mechanism and elimination strategy. J Mater Res Technol. 2025;36:7125–7134. doi:10.1016/j.jmrt.2025.04.326
[15] Pauza J, Rollett A. Simulation study of hatch spacing and layer thickness effects on microstructure in laser powder bed fusion additive manufacturing using a texture-aware solidification potts model. J Mater Eng Perform. 2021;30(9):7007–7018. doi:10.1007/s11665-021-06110-7
[16] Zhu JN, Borisov E, Liang X, et al. Controlling microstructure evolution and phase transformation behavior in additive manufacturing of nitinol shape memory alloys by tuning hatch distance. J Mater Sci. 2022;57(10):6066–6084. doi:10.1007/s10853-022-07007-z
[17] Lu N, Lei Z, Hu K, et al. Hot cracking behavior and mechanism of a third-generation Ni-based single-crystal superalloy during directed energy deposition. Addit Manuf. 2020;34:101228. doi:10.1016/j.addma.2020.101228
[18] Zhou Z, Lei Q, Yan Z, et al. Effects of process parameters on microstructure and cracking susceptibility of a single crystal superalloy fabricated by directed energy deposition. Mater Des. 2021;198:109296. doi:10.1016/j.matdes.2020.109296
[19] Manvatkar V, De A, DebRoy T. Spatial variation of melt pool geometry, peak temperature and solidification parameters during laser assisted additive manufacturing process. Mater Sci Technol. 2015;31(8):924–930. doi:10.1179/1743284714Y.0000000701
[20] Chen K, Huang R, Li Y, et al. Rafting-enabled recovery avoids recrystallization in 3D-printing-repaired single-crystal superalloys. Adv Mater. 2020;32(12):1907164. doi:10.1002/adma.201907164
[21] Lin S, Chen K, He W, et al. Custom-designed heat treatment simultaneously resolves multiple challenges facing 3D-printed single-crystal superalloys. Mater Des. 2022;222:111075. doi:10.1016/j.matdes.2022.111075
[22] Rappaz M, David SA, Vitek JM, et al. Development of microstructures in Fe-15Ni-15Cr single crystal electron beam welds. Metall Trans A. 1989;20(6):1125–1138. doi:10.1007/BF02650147
[23] Liu W, DuPont JN. Effects of substrate crystallographic orientations on crystal growth and microstructure development in laser surface-melted superalloy single crystals. Mathematical modeling of single-crystal growth in a melt pool (Part II). Acta Mater. 2005;53(5):1545–1558. doi:10.1016/j.actamat.2004.12.007
[24] Liu W, DuPont JN. Effects of melt-pool geometry on crystal growth and microstructure development in laser surface-melted superalloy single crystals: mathematical modeling of single-crystal growth in a melt pool (part I). Acta Mater. 2004;52(16):4833–4847. doi:10.1016/S1359-6454(04)00390-8
[25] Anderson TD, DuPont JN, DebRoy T. Origin of stray grain formation in single-crystal superalloy weld pools from heat transfer and fluid flow modeling. Acta Mater. 2010;58(4):1441–1454. doi:10.1016/j.actamat.2009.10.051
[26] Liang YJ, Wang HM. Origin of stray-grain formation and epitaxy loss at substrate during laser surface remelting of single-crystal nickel-base superalloys. Mater Des. 2016;102:297–302. doi:10.1016/j.matdes.2016.04.051
[27] Read WT, Shockley W. Dislocation models of crystal grain boundaries. Phys Rev. 1950;78(3):275–289. doi:10.1103/PhysRev.78.275
[28] Lin S, Chen K, Zeng Q, et al. A method for increasing the supersolvus critical strain for recrystallization in single-crystal superalloys. Mater Res Lett. 2023;11(10):856–862. doi:10.1080/21663831.2023.2253267
[29] Zhang H, Chen K, Lin S, et al. Recovery facilitated by interphase boundary motion circumvents recrystallization in superalloy single crystals. Mater Res Lett. 2024;12(3):180–189. doi:10.1080/21663831.2024.2312146

[30] Alabort E, Barba D, Sulzer S, et al. Grain boundary properties of a nickel-based superalloy: characterisation and modelling. Acta Mater. 2018;151:377–394. doi:10.1016/j.actamat.2018.03.059
[31] Horst OM, Adler D, Git P, et al. Exploring the fundamentals of Ni-based superalloy single crystal (SX) alloy design: chemical composition vs. microstructure. Mater Des. 2020;195:108976. doi:10.1016/j.matdes.2020.108976
[32] Chen L, Zhang B, Yang Y, et al. Evolution of hot processing map and microstructure of as-forged nickel-based superalloy during hot deformation. J Mater Res Technol. 2023;24:7638–7653. doi:10.1016/j.jmrt.2023.05.060
[33] Xing L, Huang H, Hao S, et al. Architecting equiaxed grain structures of additively manufactured Ni-based superalloys via heterogeneous nucleation on Nano-TiC. J Alloys Compd. 2026: 186707. doi:10.1016/j.jallcom.2026.186707
[34] Wei B, Liu Z, Cao B, et al. Cracking inhibition of nano-TiC reinforced René 104 superalloy fabricated by selective laser melting. J Alloys Compd. 2021;881:160413. doi:10.1016/j.jallcom.2021.160413
[35] Polozov I, Zolotarev A, Barabash A, et al. Effects of titanium diboride nanoparticles on the microstructure and mechanical properties of VZh159 nickel-based superalloy fabricated using selective laser melting. Mater Sci Addit Manuf. 2025;4(4):025220043. doi:10.36922/MSAM025220043
[36] Yang M, Wang L, Yan W. Phase-field modeling of grain evolutions in additive manufacturing from nucleation, growth, to coarsening. Npj Comput Mater. 2021;7(1):56. doi:10.1038/s41524-021-00524-6
[37] Fan D, Chen LQ, Chen SPP. Numerical simulation of zener pinning with growing second-phase particles. J Am Ceram Soc. 1998;81(3):526–532. doi:10.1111/j.1151-2916.1998.tb02370.x
[38] Chang K, Feng W, Chen LQ. Effect of second-phase particle morphology on grain growth kinetics. Acta Mater. 2009;57(17):5229–5236. doi:10.1016/j.actamat.2009.07.025